ELECTROMAGNETISM

Interface-driven topological Hall effect in $SrRuO_3$-$SrIrO_3$ bilayer

10.1126/sciadv.1600304

Jobu Matsuno,[1]* Naoki Ogawa,[1] Kenji Yasuda,[2] Fumitaka Kagawa,[1] Wataru Koshibae,[1] Naoto Nagaosa,[1,2] Yoshinori Tokura,[1,2] Masashi Kawasaki[1,2]

Electron transport coupled with magnetism has attracted attention over the years. Among them, recently discovered is topological Hall effect (THE), originating from scalar spin chirality, that is, the solid angle subtended by the spins. THE is found to be a promising tool for probing the Dzyaloshinskii-Moriya (DM) interaction and consequent magnetic skyrmions. This interaction arises from broken inversion symmetry and hence can be artificially introduced at interface; this concept is lately verified in metal multilayers. However, there are few attempts to investigate such DM interaction at interface through electron transport. We clarified how the transport properties couple with interface DM interaction by fabricating the epitaxial oxide interface. We observed THE in epitaxial bilayers consisting of ferromagnetic $SrRuO_3$ and paramagnetic $SrIrO_3$ over a wide region of both temperature and magnetic field. The magnitude of THE rapidly decreases with the thickness of $SrRuO_3$, suggesting that the interface DM interaction plays a significant role. Such interaction is expected to realize a 10-nm-sized Néel-type magnetic skyrmion. The present results established that the high-quality oxide interface enables us to tune the effective DM interaction; this can be a step toward future topological electronics.

INTRODUCTION

In the past several decades, electron transport intertwined with magnetism has been a focus of intensive research for its basic scientific importance as well as its possible technological applications. Anomalous Hall effect (AHE), which is driven by magnetization (M) in ferromagnets, is one of the phenomena of interest (*1*–*4*). Although ordinary Hall effect is a consequence of Lorentz force and, hence, is proportional to magnetic field (H), the origin of intrinsic AHE has been clarified to be a Berry phase in momentum space in most cases. The other type of unconventional Hall effect that is proportional to neither H nor M has recently been found in a pyrochlore ferromagnet $Nd_2Mo_2O_7$; the Hall effect has been originating from scalar spin chirality $\chi_{ijk} = \mathbf{S}_i \cdot (\mathbf{S}_j \times \mathbf{S}_k)$, which is generated by the noncoplanar configuration of Mo spins (*5*). This can be attributed to the Berry phase in real space and therefore is termed topological Hall effect (THE). Now, it is widely known that THE has been observed as well in metallic magnets that host magnetic skyrmions (see Fig. 1B), which are topologically protected nanometer-sized spin swirling textures endowed with scalar spin chirality (*6*–*10*). Among them, what is particularly important is the one formed by the Dzyaloshinskii-Moriya (DM) interaction, giving rise to smaller skyrmions with sizes of 5 to 100 nm; skyrmion-driven THE has been reported for metallic magnets with chiral crystal structure, such as that of B20 compounds (*11*–*13*), demonstrating that THE is a promising tool for probing the skyrmion.

Considering that DM interaction arises from spin-orbit coupling combined with broken inversion symmetry, it is possible to artificially introduce DM interaction at the surface/interface. This concept is indeed verified at the interface between 3*d* ferromagnetic metal (Mn, Fe, and Co) and 5*d* paramagnetic metal (W and Ir) by surface-sensitive techniques, such as spin-polarized scanning tunneling microscopy and spin-polarized low-energy electron microscopy; chirality of surface magnetism has been reported (*14*–*16*). Here, we investigate the interface DM interaction by measuring the THE. Given that high-quality epitaxial interfaces have been extensively investigated in various perovskite-type transition-metal oxides during the last decade (*17*), we combined two transition-metal oxides in the form of epitaxial bilayers of perovskite: one is $SrRuO_3$, a well-known itinerant ferromagnet with a Curie temperature (T_C) of ~160 K (*18*), and the other is $SrIrO_3$, a paramagnetic semimetal that has been lately clarified to host 5*d* electrons with strong spin-orbit coupling (*19*). The interface between $SrRuO_3$ and $SrIrO_3$ offers an ideal arena to search for the DM interaction due to the broken inversion symmetry for the following reasons: (i) there is no charge transfer due to the polar catastrophe (*20*) because it contains common A site ion (Sr^{2+}) with stable valence B site ions Ru^{4+} and Ir^{4+}, and (ii) the lattice mismatch at the interface is quite small (0.48%); the average lattice constants are 0.3923 nm (*21*) and 0.3942 nm (*22*), respectively. The studied structure is schematically depicted in Fig. 1C. We used the bilayer consisting of m unit cells of $SrRuO_3$ and two unit cells of $SrIrO_3$. At the interface, we can expect the finite DM vector pointing the in-plane direction, which may give rise to a Néel-type magnetic skyrmion (*23*–*32*). We have observed THE only when m is as small as 4 to 6, suggesting that it is derived from interface DM interaction.

RESULTS

Basic physical properties of the $SrRuO_3$-$SrIrO_3$ bilayers

Epitaxial bilayers consisting of $SrRuO_3$ and $SrIrO_3$ were deposited on $SrTiO_3$(001) substrates by pulsed laser deposition. Interface quality was examined by an atomically resolved HAADF (high-angle annular dark field)–STEM (scanning transmission electron microscopy) with enhanced atomic number contrast, as shown in Fig. 1C; two layers of Ir atoms indicated by the brightest spots are accurately aligned in the [001] plane, manifesting the abrupt interface. The bilayer samples were further

[1]RIKEN Center for Emergent Matter Science (CEMS), Saitama 351-0198, Japan. [2]Department of Applied Physics, University of Tokyo, Tokyo 113-8656, Japan.
*Corresponding author. Email: matsuno@riken.jp

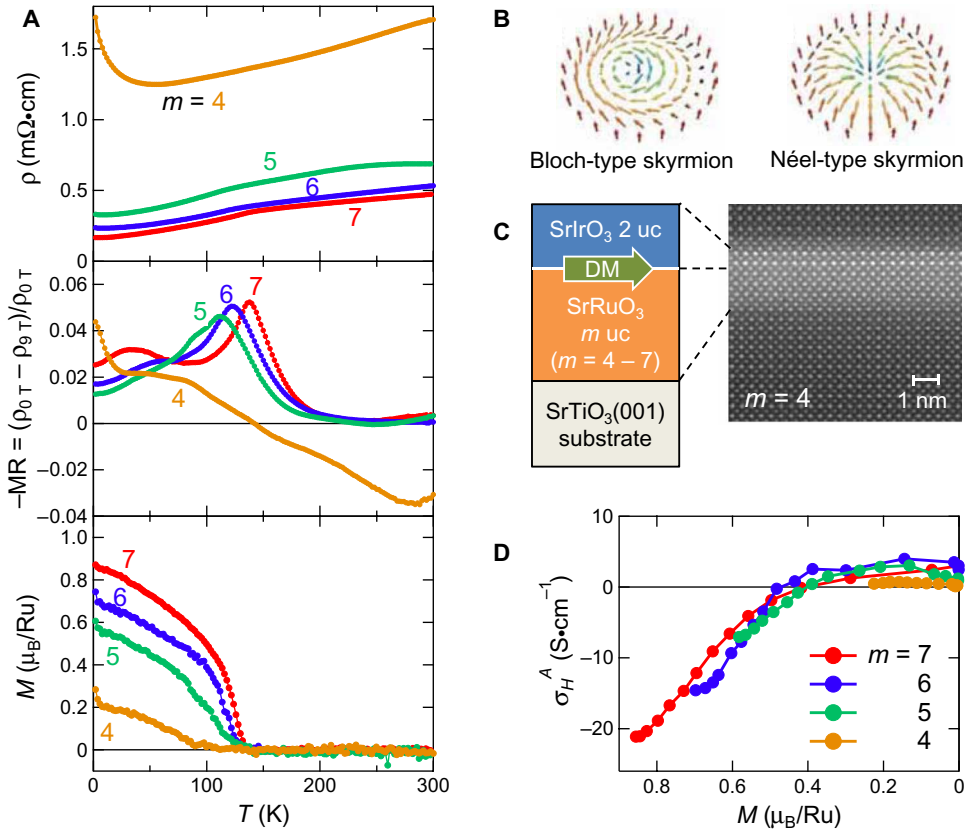

Fig. 1. Structure and basic physical properties of the $SrRuO_3$-$SrIrO_3$ bilayers. (**A**) Temperature (*T*) dependence of resistivity (ρ, top panel), MR (middle panel), and out-of-plane magnetization measured at 0.05 T (bottom panel) for the $(SrRuO_3)_m$-$(SrIrO_3)_2$ bilayers (*m* = 4, 5, 6, and 7). (**B**) Schematics of Bloch- and Néel-type skyrmions. (**C**) Schematics and an atomically resolved HAADF-STEM image of the studied bilayer structure. In the STEM image, $SrTiO_3$ is capped on top of the $SrIrO_3$ layer to protect the surface from electron beam radiation. uc, unit cells. (**D**) Anomalous Hall conductance (σ_H^A) as a function of magnetization (*M*), which was varied through temperature.

characterized by transport and magnetic measurements as displayed in Fig. 1A. The resistivity decreases systematically with *m*. Whereas the samples with $m \geq 5$ have resistivity less than 1 milliohm·cm and metallic temperature dependence, the *m* = 4 bilayer has particularly higher resistivity with a small upturn below 50 K. These indicate that the electrons in the bilayers tend to be localized with decreasing *m*, reaching to the nearly insulating state at *m* = 4. The magnetoresistance (MR) also suggests that the ferromagnetic state is relatively destabilized with decreasing *m*, as can be seen in the systematic shift of the MR peaks that are known to correspond to T_C. The magnetization clearly evidences that both the saturated moment and the T_C are suppressed for smaller *m*; the T_C almost reaches down to 90 K at *m* = 4. This is naturally expected because the ferromagnetism of $SrRuO_3$ is driven by its itinerant properties. The same trend has been reported for ultrathin $SrRuO_3$ films (*33*). To see more closely the *m*-dependent evolution of the transport and magnetic properties, we measured AHE (details of AHE as a function of magnetic field are discussed later). Anomalous Hall conductance is plotted as a function of magnetization in Fig. 1D, demonstrating both the sign change and the good scaling with variation of *M*. The preceding studies reported on the same scaling behavior, which have been attributed to the actions of momentum-space monopoles in the band structure of $SrRuO_3$ (*34*, *35*). Therefore, the observed scaling relationship indicates that the magnetic transport properties of the bilayers are governed by those of $SrRuO_3$. The systematics found in resistivity, MR, and AHE reveals that the samples are precisely controlled by *m*, the thickness of $SrRuO_3$.

Anomaly in Hall resistivity: THE

We observed the clear anomaly in the Hall resistivity only in the case of small *m*. Figure 2A shows the Hall resistivity of the bilayers as a function of magnetic field. In *m* = 4, we can clearly see the unconventional behavior of the Hall resistivity below 60 K, whereas the overall lineshape is dominated by the positive AHE. At 5 K, for example, the red curve indicates the hump structure between 0.8 and 2.1 T with increasing magnetic field. When we reverse the sweep direction, in contrast, the data drawn in blue are monotonic in the same field range. In general, Hall resistivity is expressed by

$$\rho_H = R_0 H + R_S M + \rho_H^T$$

where the first, second, and third terms denote the ordinary Hall effect, AHE, and THE, respectively. Here, we neglect the first term that is already subtracted from the data in Fig. 2. The observed nonmonotonic

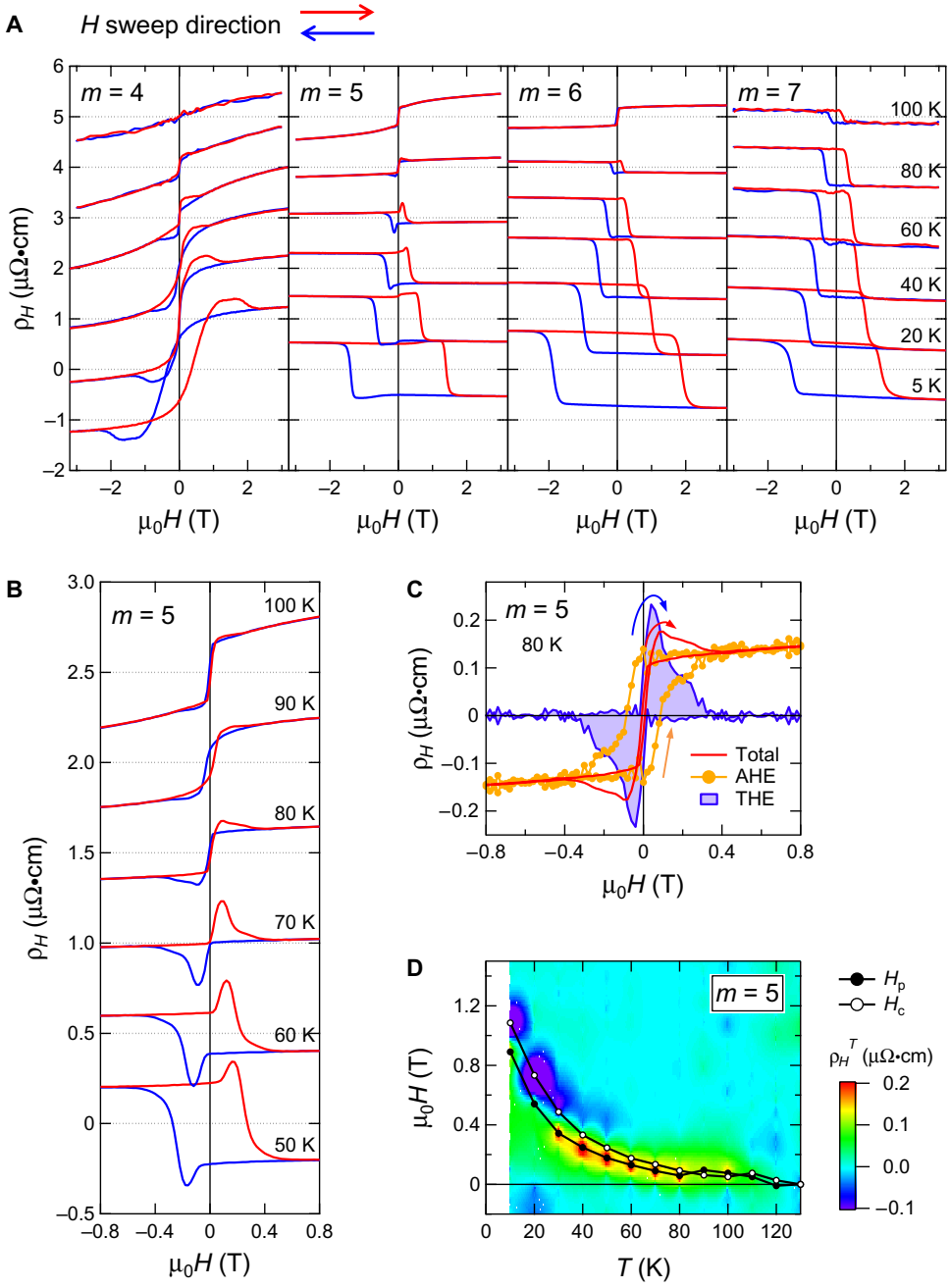

Fig. 2. Hall resistivity of all the bilayers. (**A**) Magnetic field dependence of Hall resistivity (ρ_H) of the $(SrRuO_3)_m$-$(SrIrO_3)_2$ bilayers (m = 4, 5, 6, and 7) at various temperatures. Red and blue represent sweep directions of magnetic field. Ordinary Hall term is subtracted by the linear fitting in a higher magnetic field region. (**B**) Detailed view of the Hall resistivity of m = 5. (**C**) Contribution from AHE and THE of m = 5 at 80 K (see text for details). (**D**) Color map of topological Hall resistivity in the T-H plane for m = 5. Black open and filled symbols represent coercive field (H_c) and the field at which topological Hall resistivity reaches its maximum (H_p), respectively.

hump structure can never be attributed to the magnetization (M-H) curve; we can assign the structure to the third term THE. Increasing the thickness m to 5, we can still discern the similar peak structure. To more clearly demonstrate it, the magnified view of the detailed temperature dependence is presented in Fig. 2B. At lower temperatures of 60 K, ρ_H drawn in red consists of negative AHE and an additional peak at around 0.15 T. AHE goes across zero at 70 K, at which Hall resistivity accidentally provides the genuine topological Hall component; it represents its maximum at 0.1 T. At 80 and 90 K, we can detect THE with positive AHE, giving rise to the similar lineshape with m = 4. In m = 6, a very tiny THE is discerned, whereas it is indistinguishable in the scale of Fig. 2A. Eventually, we do not observe any unconventional feature for m = 7.

To precisely evaluate THE, we separated AHE and THE by measuring the Kerr rotation angle; the Kerr signal magnitude is anticipated to be proportional to M and, hence, AHE as a function of magnetic field at a fixed temperature (see section SI in the Supplementary Materials for comparison between the Kerr rotation angle and the magnetization). The representative data set of $m = 5$ at 80 K is plotted in Fig. 2C. At the high magnetic field region where the magnetization is saturated, all the spins align ferromagnetically, leading to the absence of scalar spin chirality; the Hall resistivity is attributed only to AHE. Then, we can fit the Hall resistivity by using the Kerr rotation angle to obtain AHE. Figure 2C establishes that the fitting is quite well performed, illustrating that we can obtain THE by subtracting AHE from the total Hall resistivity. The resultant THE in Fig. 2C has a very similar lineshape with that of the 70-K data in Fig. 2B discussed above, indicating that the subtraction procedure works well. Increasing the field from −9 to 0 T, the magnetic state is totally dominated by ferromagnetic state with negative magnetization. This corresponds to the observed finite AHE and the negligible THE. With further increase of the magnetic field from 0 to 0.8 T, THE abruptly takes a peak at 0.06 T and gradually decreases to zero at 0.4 T, which coincides with the field at which the hysteresis in M-H curve closes. This suggests that some specific spin structure with finite scaler spin chirality is induced when the ferromagnetic spins begin to be reversed. The simultaneous observation of the hysteresis and the THE indicates a coexistence between the ferromagnetic phase and the phase with scalar spin chirality. We also note that the scalar spin chirality was observed only by the transport property through the emergent magnetic field, that is, a fictitious magnetic field derived from the real-space Berry phase, whereas the chirality only marginally affects the magnetization.

We applied the same procedure to all the data shown in Fig. 2A to obtain the topological Hall term as functions of both T and H. As clearly exemplified in Fig. 2D for $m = 5$, a sign of THE is always positive, irrespective of the sign change of AHE at 70 K. Although we can recognize the negative ρ_H^T in the vicinity of the coercive field (H_c) at lower temperatures, we have some experimental uncertainty there because the dominating anomalous term changes very abruptly at H_c. The observed positive THE thus indicates that it has a totally different origin from AHE. Instead, we confirm again that THE is driven by the magnetization reversal process because the peak position of ρ_H^T (H_p) scales quite well with H_c. We also note that the topological Hall term is observed in the wide range of the T-H plane. The most plausible spin-chiral structure responsible for THE is the magnetic skyrmion. In the bulk B20 compounds, the lattice form of skyrmions (Bloch type, Fig. 1B) was found in a very narrow T-H window close to T_C (*7*). In contrast, thin films of B20 compounds are reported to stabilize the skyrmion, which is discussed in terms of the film thickness relative to the skyrmion size (*9*, *13*). In our case of ultrathin $SrRuO_3$ films with roughly 2-nm thickness, we can reasonably expect the stability of the two-dimensional skyrmion, which is consistent with the observed wide-range THE.

Ferromagnet thickness dependence of THE

We now clarify the importance of interface from the m dependence of the topological Hall term. Figure 3A plots $\rho_H^T(m, T)$, the maximum value of the topological Hall term at $H = H_p$, signifying that it decreases with m, ending up with complete disappearance at $m = 7$. This m dependence can be qualitatively explained by assuming the DM vector only at the interface. To realize spin texture with finite spin chirality, all the spins of $SrRuO_3$ through the thickness should be twisted by the interface DM interaction; the energy cost for twisting the same angle linearly scales with m, that is, volume of the ferromagnet, as shown in schematics in the bottom panel of Fig. 3A. In other words, effective DM interaction ($\equiv D_{\mathrm{eff}}$) is expected to decrease with m. For a more precise understanding, we performed the following two-step analysis: (i) to investigate D_{eff} as a function of m and (ii) to estimate the energetics of two-dimensional skyrmion with D_{eff}.

To elucidate the m dependence of the effective DM interaction, we numerically examined a single skyrmion stability in a multilayer system modeled by the following Hamiltonian (see section SII in the Supplementary Materials for details of the calculation)

$$H = -J \sum_{\langle li l' i' \rangle} \boldsymbol{n}_{l,i} \cdot \boldsymbol{n}_{l',i'} + D \sum_{i} [\hat{\boldsymbol{y}} \cdot (\boldsymbol{n}_{1,i} \times \boldsymbol{n}_{1,i+\hat{x}}) - \hat{\boldsymbol{x}} \cdot (\boldsymbol{n}_{1,i} \times \boldsymbol{n}_{1,i+\hat{y}})] - h \sum_{l=1}^{m} \sum_{i} \boldsymbol{n}_{l,i}^{z}$$

where J is the ferromagnetic coupling constant and D is the DM interaction only on the first layer ($l = 1$). The normalized magnetic moment at the site $\boldsymbol{i}$ on the layer l is denoted as $\boldsymbol{n}_{l,i}$. The unit vectors $\hat{\boldsymbol{x}}$ and $\hat{\boldsymbol{y}}$ define the two-dimensional square lattice on a layer. The last term represents the Zeeman energy with external magnetic field h perpendicular to the multilayer. Control parameters are D, and total number of layers is m, whereas we fix $J = 1.0$ and $h = 0.01$. Through the whole parameter range, we obtained three types of magnetic structures: helix, single skyrmion, and perfect ferromagnet. In the right panel of Fig. 3C, we have shown the typical real-space patterns for the helix and the skyrmion, indicating that the skyrmion is of Néel type as expected in the interface systems (*23*–*32*). We also note that the skyrmion is nearly cylindrical, that is, its radius is almost independent of the layers (see section SII in the Supplementary Materials for details). The left panel of Fig. 3C shows the stability of the above three magnetic structures, clearly demonstrating that the skyrmion state is realized under larger D and smaller m than the ferromagnetic state. For instance, at $D = 0.3$, the cylindrical Néel-type skyrmion ($m \leq 6$) and the ferromagnet ($m \geq 7$) are stabilized, as depicted in the schematics of Fig. 3A. This is consistent with the experimental result showing the emergence of THE in smaller m ($m \leq 6$) for a given D at the $SrRuO_3$-$SrIrO_3$ interface. Thus, we can conclude that THE in our bilayers stems from the interface DM interaction and the resultant Néel-type skyrmions. We also find that the stable regions for the single skyrmion and the ferromagnetic state are divided by an almost linear function of m. This is understood by introducing $D_{\mathrm{eff}} = D/m$ as follows. Because of the cylindrical nature of the skyrmion mentioned above, the magnetic moments $\boldsymbol{n}_{l,i}$ are almost parallel to each other between layers. The total intralayer ferromagnetic interaction is, thus, just m times as large as that of the single layer, equivalent to the scale-down of the effective DM interaction given by $D_{\mathrm{eff}} = D/m$.

With the obtained D_{eff}, we discuss more detailed energetics in a two-dimensional ferromagnet described by parameters D_{eff}, J, and K, where K denotes the anisotropy constant. Because $SrRuO_3$ is a ferromagnet with perpendicular easy axis, both J and K are positive. In this situation, it is known that these parameters can be reduced to a single parameter, $\kappa = \sqrt{D_{\mathrm{eff}}^2/(JK)}$, to describe the magnetostatics; the sign of D_{eff} does not change the energetics while it determines the helicity of the skyrmion (*36*, *37*). In the theory considering both the magnetocrystalline

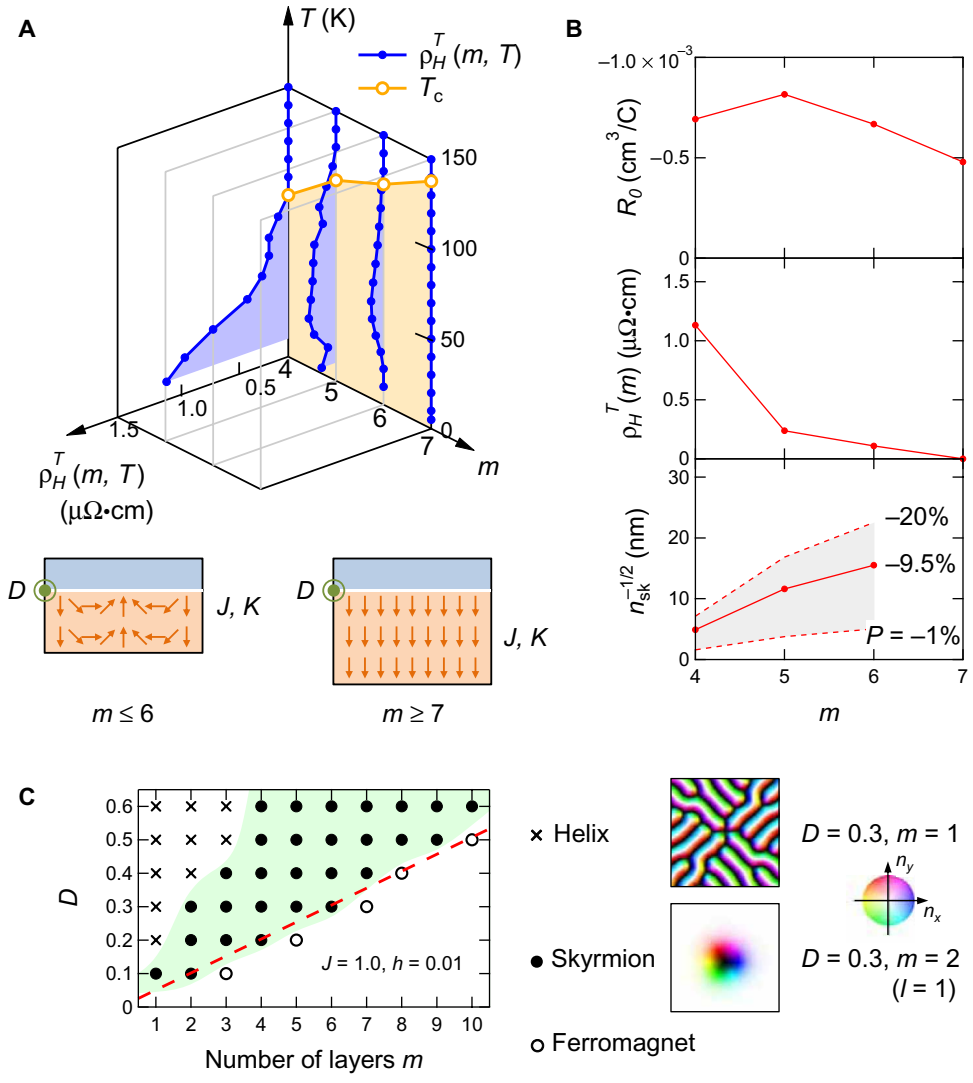

Fig. 3. THE and calculated stability of skyrmions as a function of the ferromagnet thickness. (**A**) Topological Hall resistivity as functions of *m* and *T*. T_C of the bilayers is also shown. The schematics below indicate the relationship between the spin structure and interface DM interaction depending on $SrRuO_3$ thickness. (**B**) *m* dependence of the ordinary Hall coefficient (R_0, top panel), the maximum of the topological Hall resistivity in the *T*-*H* plane [$\rho_H^T(m)$, middle panel], and the inverse of the square root of the possible skyrmion density ($n_{sk}^{-1/2}$, bottom panel). (**C**) Calculated phase diagram of the stable magnetic structures as functions of *m* and *D*. We have obtained three types of the magnetic structures, namely, helix, skyrmion, and perfect ferromagnet. For the former two, we also show the typical real-space patterns in the right panel. The image size is 150 × 150 unit cells.

anisotropy and the dipolar interaction, there is a critical value in κ that differentiates the skyrmion phase and the ferromagnetic phase; the former is favored for larger κ (*36*, *37*), which corresponds to a smaller *m* in our case. In $SrRuO_3$, *K* is reported to be 0.64 J · cm^{-2} (*38*). If we assume that bulk $SrRuO_3$ is a three-dimensional Heisenberg ferromagnet with $S = 1$, *J* is expected to be (3/2) T_C = 240 K in the mean-field approximation. Because the critical value of κ is about unity (*36*, *37*), the effective magnitude of the DM vector $|D_{eff}|$ should be close to $\sqrt{JK}$ = 2.3 meV to stabilize the skyrmion state for the $m \leq 6$ samples. The real $|D|$ value defined at the interface is thus deduced to be $m|D_{eff}|$ = 14 meV. This is much larger than those in the interface between metals: −2.2 meV for permalloy/Pt (*39*) and −1.05 meV for a Co/Ni multilayer on Pt(111) (*16*).

In the skyrmion systems, a single skyrmion can be regarded as one flux quantum ($\phi_0 = h/e$, where *h* is the Planck constant and *e* is the elementary charge) in the limit of strong spin-charge coupling. The skyrmion density (n_{sk}) then gives rise to the emergent magnetic field (*b*) as $b = n_{sk}\phi_0$. The topological Hall resistivity is hence represented by the following formula

$$\rho_H^T = PR_0 b = PR_0 n_{sk}\phi_0$$

where *P* denotes the spin polarization of conduction electron in $SrRuO_3$. Because *P* is found to be −9.5% by the tunneling MR in a junction with a 50-nm-thick $SrRuO_3$ (*40*), we can deduce n_{sk}. To

roughly estimate the separation of the skyrmions, we plotted $n_{sk}^{-1/2}$ in Fig. 3B, with $\rho_H^T(m)$ as the maximum of the topological Hall resistivity in the T-H plane and R_0 as a function of m. Because there is some uncertainty whether the spin polarization value of −9.5% can be applied to our ultrathin $SrRuO_3$ films, we also appended $n_{sk}^{-1/2}$ for $P = -1$ and −20%. We can approximately estimate that the separation of skyrmions ($n_{sk}^{-1/2}$) is 10 to 20 nm in our bilayers. This is an area-averaged value; its increase with m corresponds to the instability of the skyrmion phase as already discussed. Considering the abovementioned coexistence between the skyrmion and the ferromagnetic phase, the local interskyrmion spacing can be even smaller. Nevertheless, the $n_{sk}^{-1/2}$ value of 10 to 20 nm still provides an indication of the length scale of the skyrmion because its lower limit should be larger than the film thickness of ~2 nm because of the two-dimensional nature of the skyrmion. We also note that this value is comparable to that of the bulk B20 compounds and therefore is promising as well in terms of possible recording memory density (*41*). The result indicates that the interface DM interaction at the oxide heterojunction is one of the promising ways to produce skyrmions. This functionality is achieved only by the atomically flat oxide interfaces endowed with high tunability.

DISCUSSION

We have observed THE in the $SrRuO_3$-$SrIrO_3$ bilayers. By investigating the ferromagnet thickness dependence, we have demonstrated that the skyrmion phase is driven by the interface DM interaction as a consequence of both the broken inversion symmetry and strong spin-orbit coupling of $SrIrO_3$. The result provides a basis for designing and controlling the interface-driven skyrmions in nonchiral magnets, which should be indispensable to future topological electronics. To fully elucidate the nature of the interface DM interaction, further studies on real space observation of skyrmions will be needed. In section SIII in the Supplementary Materials, we show the preliminary result of magnetic force microscopy for the $m = 5$ sample, which is compatible with the skyrmion picture described here. Also useful is the direct measurement of the interface DM vector by means of Brillouin light scattering or ferromagnetic resonance (*39*, *42*–*44*).

MATERIALS AND METHODS

Sample fabrication

Epitaxial bilayers consisting of $SrRuO_3$ and $SrIrO_3$ were deposited on $SrTiO_3$(001) substrates by pulsed laser deposition using a KrF excimer laser (λ = 248 nm) with a fluence of 1 to 2 J/cm^2 on the target surface. The oxygen partial pressure and deposition temperature were optimized at 13 Pa and 680°C for $SrRuO_3$ and at 19 Pa and 610°C for $SrIrO_3$, respectively.

Measurements

The magnetization data were recorded by SQUID magnetometer with a magnetic field applied perpendicularly to the film plane because the magnetic easy axis of the $SrRuO_3$ film is perpendicular to the film plane when grown on $SrTiO_3$(001) (*45*). Magneto-optic Kerr effect was measured with a laser at 690 nm in polar geometry by using a photoelastic modulator. In transport measurements, we applied 3 μA to a Hall bar with width of 400 μm and length of 1000 μm. This corresponds to the current density of ~3 × 10^2 A·cm^{-2} in the case of m = 4. Antisymmetrization was performed for both the Hall resistivity and the Kerr rotation angle. Ordinary Hall term was subtracted from the Hall resistivity by linear fitting in a higher magnetic field region.

SUPPLEMENTARY MATERIALS

Supplementary material for this article is available at http://advances.sciencemag.org/cgi/content/full/2/7/e1600304/DC1

section SI. Comparison between the Kerr rotation angle and the magnetization

section SII. Details of the calculation of the skyrmion stability in the multilayer

section SIII. Preliminary magnetic force microscopy images

fig. S1. Kerr rotation, magnetization, and topological Hall resistivity.

fig. S2. Multilayer model and calculated skyrmion radius.

fig. S3. Magnetic force microscopy images for m = 5 measured at 50 K and various magnetic field.

REFERENCES AND NOTES

1. N. Nagaosa, J. Sinova, S. Onoda, A. H. MacDonald, N. P. Ong, Anomalous Hall effect. *Rev. Mod. Phys.* **82**, 1539–1592 (2010).
2. J. Ye, Y. B. Kim, A. J. Millis, B. I. Shraiman, P. Majumdar, Z. Tešanović, Berry phase theory of the anomalous Hall effect: Application to colossal magnetoresistance manganites. *Phys. Rev. Lett.* **83**, 3737–3740 (1999).
3. M. Onoda, G. Tatara, N. Nagaosa, Anomalous Hall effect and skyrmion number in real and momentum spaces. *J. Phys. Soc. Jpn.* **73**, 2624–2627 (2004).
4. P. Bruno, V. K. Dugaev, M. Taillefumier, Topological Hall effect and Berry phase in magnetic nanostructures. *Phys. Rev. Lett.* **93**, 096806 (2004).
5. Y. Taguchi, Y. Oohara, H. Yoshizawa, N. Nagaosa, Y. Tokura, Spin chirality, Berry phase, and anomalous Hall effect in a frustrated ferromagnet. *Science* **291**, 2573–2576 (2001).
6. U. K. Rößler, A. N. Bogdanov, C. Pfleiderer, Spontaneous skyrmion ground states in magnetic metals. *Nature* **442**, 797–801 (2006).
7. S. Mühlbauer, B. Binz, F. Jonietz, C. Pfleiderer, A. Rosch, A. Neubauer, R. Georgii, P. Böni, Skyrmion lattice in a chiral magnet. *Science* **323**, 915–919 (2009).
8. X. Z. Yu, Y. Onose, N. Kanazawa, J. H. Park, J. H. Han, Y. Matsui, N. Nagaosa, Y. Tokura, Real-space observation of a two-dimensional skyrmion crystal. *Nature* **465**, 901–904 (2010).
9. X. Z. Yu, N. Kanazawa, Y. Onose, K. Kimoto, W. Z. Zhang, S. Ishiwata, Y. Matsui, Y. Tokura, Near room-temperature formation of a skyrmion crystal in thin-films of the helimagnet FeGe. *Nat. Mater.* **10**, 106–109 (2011).
10. N. Nagaosa, Y. Tokura, Topological properties and dynamics of magnetic skyrmions. *Nat. Nanotechnol.* **8**, 899–911 (2013).
11. A. Neubauer, C. Pfleiderer, B. Binz, A. Rosch, R. Ritz, P. G. Niklowitz, P. Böni, Topological Hall effect in the *A* phase of MnSi. *Phys. Rev. Lett.* **102**, 186602 (2009).
12. N. Kanazawa, Y. Onose, T. Arima, D. Okuyama, K. Ohoyama, S. Wakimoto, K. Kakurai, S. Ishiwata, Y. Tokura, Large topological Hall effect in a short-period helimagnet MnGe. *Phys. Rev. Lett.* **106**, 156603 (2011).
13. T. Yokouchi, N. Kanazawa, A. Tsukazaki, Y. Kozuka, M. Kawasaki, M. Ichikawa, F. Kagawa, Y. Tokura, Stability of two-dimensional skyrmions in thin films of $Mn_{1-x}Fe_xSi$ investigated by the topological Hall effect. *Phys. Rev. B* **89**, 064416 (2014).
14. M. Bode, M. Heide, K. von Bergmann, P. Ferriani, S. Heinze, G. Bihlmayer, A. Kubetzka, O. Pietzsch, S. Blügel, R. Wiesendanger, Chiral magnetic order at surfaces driven by inversion asymmetry. *Nature* **447**, 190–193 (2007).
15. N. Romming, A. Kubetzka, C. Hanneken, K. von Bergmann, R. Wiesendanger, Field-dependent size and shape of single magnetic skyrmions. *Phys. Rev. Lett.* **114**, 177203 (2015).
16. G. Chen, T. Ma, A. T. N'Diaye, H. Kwon, C. Won, Y. Wu, A. K. Schmid, Tailoring the chirality of magnetic domain walls by interface engineering. *Nat. Commun.* **4**, 2671 (2013).
17. H. Y. Hwang, Y. Iwasa, M. Kawasaki, B. Keimer, N. Nagaosa, Y. Tokura, Emergent phenomena at oxide interfaces. *Nat. Mater.* **11**, 103–113 (2012).
18. G. Koster, L. Klein, W. Siemons, G. Rijnders, J. S. Dodge, C.-B. Eom, D. H. A. Blank, M. R. Beasley, Structure, physical properties, and applications of $SrRuO_3$ thin films. *Rev. Mod. Phys.* **84**, 253–298 (2012).
19. J. Matsuno, K. Ihara, S. Yamamura, H. Wadati, K. Ishii, V. V. Shankar, H.-Y. Kee, H. Takagi, Engineering a spin-orbital magnetic insulator by tailoring superlattices. *Phys. Rev. Lett.* **114**, 247209 (2015).
20. N. Nakagawa, H. Y. Hwang, D. A. Muller, Why some interfaces cannot be sharp. *Nat. Mater.* **5**, 204–209 (2006).
21. C. W. Jones, P. D. Battle, P. Lightfoot, W. T. A. Harrison, The structure of $SrRuO_3$ by time-of-flight neutron powder diffraction. *Acta Crystallogr. C* **45**, 365–367 (1989).

22. J. G. Zhao, L. X. Yang, Y. Yu, F. Y. Li, R. C. Yu, Z. Fang, L. C. Chen, C. Q. Jin, High-pressure synthesis of orthorhombic $SrIrO_3$ perovskite and its positive magnetoresistance. *J. Appl. Phys.* **103**, 103706 (2008).
23. A. Fert, V. Cros, J. Sampaio, Skyrmions on the track. *Nat. Nanotechnol.* **8**, 152–156 (2013).
24. S. Heinze, K. von Bergmann, M. Menzel, J. Brede, A. Kubetzka, R. Wiesendanger, G. Bihlmayer, S. Blügel, Spontaneous atomic-scale magnetic skyrmion lattice in two dimensions. *Nat. Phys.* **7**, 713–718 (2011).
25. W. Jiang, P. Upadhyaya, W. Zhang, G. Yu, M. B. Jungfleisch, F. Y. Fradin, J. E. Pearson, Y. Tserkovnyak, K. L. Wang, O. Heinonen, S. G. E. te Velthuis, A. Hoffmann, Blowing magnetic skyrmion bubbles. *Science* **349**, 283–286 (2015).
26. C. Moreau-Luchaire, C. Moutafis, N. Reyren, J. Sampaio, C. A. F. Vaz, N. Van Horne, K. Bouzehouane, K. Garcia, C. Deranlot, P. Warnicke, P. Wohlhüter, J.-M. George, M. Weigand, J. Raabe, V. Cros, A. Fert, Additive interfacial chiral interaction in multilayers for stabilization of small individual skyrmions at room temperature. *Nat. Nanotechnol.* **11**, 444–448 (2016).
27. R. Wakatsuki, M. Ezawa, N. Nagaosa, Domain wall of a ferromagnet on a three-dimensional topological insulator. *Sci. Rep.* **5**, 13638 (2015).
28. S. Banerjee, J. Rowland, O. Erten, M. Randeria, Enhanced stability of skyrmions in two-dimensional chiral magnets with Rashba spin-orbit coupling. *Phys. Rev. X* **4**, 031045 (2014).
29. R. Keesman, A. O. Leonov, P. van Dieten, S. Buhrandt, G. T. Barkema, L. Fritz, R. A. Duine, Degeneracies and fluctuations of Néel skyrmions in confined geometries. *Phys. Rev. B* **92**, 134405 (2015).
30. U. Güngördü, R. Nepal, O. A. Tretiakov, K. Belashchenko, A. A. Kovalev, Stability of skyrmion lattices and symmetries of quasi-two-dimensional chiral magnets. *Phys. Rev. B* **93**, 064428 (2016).
31. I. Kézsmárki, S. Bordács, P. Milde, E. Neuber, L. M. Eng, J. S. White, H. M. Rønnow, C. D. Dewhurst, M. Mochizuki, K. Yanai, H. Nakamura, D. Ehlers, V. Tsurkan, A. Loidl, Néel-type skyrmion lattice with confined orientation in the polar magnetic semiconductor GaV_4S_8. *Nat. Mater.* **14**, 1116–1122 (2015).
32. S. Woo, K. Litzius, B. Krüger, M.-Y. Im, L. Caretta, K. Richter, M. Mann, A. Krone, R. M. Reeve, M. Weigand, P. Agrawal, I. Lemesh, M.-A. Mawass, P. Fischer, M. Kläui, G. S. D. Beach, Observation of room-temperature magnetic skyrmions and their current-driven dynamics in ultrathin metallic ferromagnets. *Nat. Mater.* **15**, 501–506 (2016).
33. J. Xia, W. Siemons, G. Koster, M. R. Beasley, A. Kapitulnik, Critical thickness for itinerant ferromagnetism in ultrathin films of $SrRuO_3$. *Phys. Rev. B* **79**, 140407 (2009).
34. Z. Fang, N. Nagaosa, K. S. Takahashi, A. Asamitsu, R. Mathieu, T. Ogasawara, H. Yamada, M. Kawasaki, Y. Tokura, K. Terakura, The anomalous Hall effect and magnetic monopoles in momentum space. *Science* **302**, 92–95 (2003).
35. R. Mathieu, A. Asamitsu, H. Yamada, K. S. Takahashi, M. Kawasaki, Z. Fang, N. Nagaosa, Y. Tokura, Scaling of the anomalous Hall effect in $Sr_{1-x}Ca_xRuO_3$. *Phys. Rev. Lett.* **93**, 016602 (2003).
36. A. Bogdanov, D. Yablonskii, Thermodynamically stable "vortices" in magnetically ordered crystals. The mixed state of magnets. *Zh. Eksp. Teor. Fiz* **95**, 178–182 (1989).
37. A. Bogdanov, A. Hubert, Thermodynamically stable magnetic vortex states in magnetic crystals. *J. Magn. Magn. Mater.* **138**, 255–269 (1994).
38. A. Kanbayasi, Magnetocrystalline anisotropy of $SrRuO_3$. *J. Phys. Soc. Jpn.* **41**, 1879–1883 (1976).
39. H. T. Nembach, J. M. Shaw, M. Weiler, E. Jué, T. J. Silva, Linear relation between Heisenberg exchange and interfacial Dzyaloshinskii–Moriya interaction in metal films. *Nat. Phys.* **11**, 825–829 (2015).
40. D. C. Worledge, T. H. Geballe, Negative spin-polarization of $SrRuO_3$. *Phys. Rev. Lett.* **85**, 5182–5185 (2000).
41. W. Koshibae, Y. Kaneko, J. Iwasaki, M. Kawasaki, Y. Tokura, N. Nagaosa, Memory functions of magnetic skyrmions. *Jpn. J. Appl. Phys.* **54**, 053001 (2015).
42. K. Di, V. L. Zhang, H. S. Lim, S. C. Ng, M. H. Kuok, J. Yu, J. Yoon, X. Qiu, H. Yang, Direct observation of the Dzyaloshinskii-Moriya interaction in a Pt/Co/Ni film. *Phys. Rev. Lett.* **114**, 047201 (2015).
43. J. Cho, N.-H. Kim, S. Lee, J.-S. Kim, R. Lavrijsen, A. Solignac, Y. Yin, D.-S. Han, N. J. J. van Hoof, H. J. M. Swagten, B. Koopmans, C.-Y. You, Thickness dependence of the interfacial Dzyaloshinskii–Moriya interaction in inversion symmetry broken systems. *Nat. Commun.* **6**, 7635 (2015).
44. A. A. Stashkevich, M. Belmeguenai, Y. Roussigné, S. M. Cherif, M. Kostylev, M. Gabor, D. Lacour, C. Tiusan, M. Hehn, Experimental study of spin-wave dispersion in Py/Pt film structures in the presence of an interface Dzyaloshinskii-Moriya interaction. *Phys. Rev. B* **91**, 214409 (2015).
45. L. Klein, J. S. Dodge, C. H. Ahn, J. W. Reiner, L. Mieville, T. H. Geballe, M. R. Beasley, A. Kapitulnik, Transport and magnetization in the badly metallic itinerant ferromagnet $SrRuO_3$. *J. Phys. Condens. Matter* **8**, 10111–10126 (1996).

Acknowledgments: We thank X. Z. Yu and O. Tretiakov for fruitful discussions. **Funding:** This work was partly supported by the "Funding Program for World-Leading Innovative R&D on Science and Technology (FIRST)" of the Japan Society for the Promotion of Science (JSPS) initiated by the Council for Science and Technology Policy. **Author contributions:** J.M. conceived the research, conducted the sample fabrication and the transport measurements, and wrote the manuscript. N.O. measured the magneto-optic Kerr effect. K.Y. and F.K. performed the magnetic force microscopy. W.K. and N.N. carried out the model calculation. Y.T. and M.K. supervised the project. All authors discussed the results. **Competing interests:** The authors declare that they have no competing interests. **Data and materials availability:** All data needed to evaluate the conclusions in the paper are present in the paper and/or the Supplementary Materials. Additional data related to this paper may be requested from the authors.

Submitted 12 February 2016
Accepted 13 June 2016
Published 8 July 2016
10.1126/sciadv.1600304

Citation: J. Matsuno, N. Ogawa, K. Yasuda, F. Kagawa, W. Koshibae, N. Nagaosa, Y. Tokura, M. Kawasaki, Interface-driven topological Hall effect in $SrRuO_3$-$SrIrO_3$ bilayer. *Sci. Adv.* **2**, e1600304 (2016).

Interface-driven topological Hall effect in $SrRuO_3$-$SrIrO_3$ bilayer

Jobu Matsuno, Naoki Ogawa, Kenji Yasuda, Fumitaka Kagawa, Wataru Koshibae, Naoto Nagaosa, Yoshinori Tokura and Masashi Kawasaki

Sci Adv **2** (7), e1600304.
DOI: 10.1126/sciadv.1600304